

KURUCZ MODEL ENERGY DISTRIBUTIONS: A COMPARISON WITH REAL STARS. II. METAL-DEFICIENT STARS

V. Straizys¹, R. Lazauskaitė^{1,2} and G. Valiauga¹

¹ *Institute of Theoretical Physics and Astronomy, Goštauto 12,
Vilnius 2600, Lithuania;*

² *Department of Theoretical Physics, Vilnius Pedagogical University,
Studentų 39, Vilnius 2340, Lithuania.*

Received July 25, 2002.

Abstract. Energy distributions of synthetic spectra for Kurucz model atmospheres are compared with observed energy distributions of metal-deficient stars of the blue horizontal-branch (BHB), F–G–K subdwarf (SD) and G–K giant (MDG) types. The best coincidence of the synthetic and observed energy curves is found for BHB stars. The largest differences are found in the ultraviolet wavelengths for subdwarfs and cool MDGs. The influence of errors of effective temperatures, gravities and metallicities is estimated.

Key words: stars: fundamental parameters, spectral energy distribution – stars: horizontal-branch, subdwarfs, metal-deficient giants

1. INTRODUCTION

Synthetic energy distributions of the Kurucz models (Kurucz 1995) are frequently used for a selection of optimum positions of passbands for multicolor photometric systems and for calculation of parameters of photometric systems or of transformation equations between color indices of different photometric systems. However, the use of synthetic spectra for these tasks is justified only in the case if the synthetic spectra of model atmospheres coincide sufficiently well with energy distributions of real stars having the same physical parameters (effective temperatures, gravities and metallicities).

In our first paper (Straizys, Liubertas & Valiauga 1997) we have compared energy distributions of the Kurucz model atmospheres with the mean energy distributions of stars of various spectral types of solar metallicity published by Straizys & Sviderskienė (1972) and revised by one of the authors. In the present paper we compare the Kurucz synthetic spectra of metal-deficient models with spectral energy distributions of real stars – blue horizontal-branch (hereafter, BHB) stars, F–G subdwarfs (hereafter, SD) and G–K metal-deficient giants (hereafter, MDG) published by Sviderskienė (1992).

2. INTRINSIC ENERGY DISTRIBUTION CURVES OF STARS

Energy distribution functions of 52 stars – 9 blue horizontal-branch stars, 11 extreme F–G–K subdwarfs, 10 mild F–G subdwarfs, 14 mild metal-deficient G–K giants and subgiants and 6 extreme metal-deficient G–K giants – were published by Sviderskienė (1992). The wavelength dependence of energy fluxes for each of these stars was determined by averaging the data from all sources found in the literature until 1990. For the majority of stars the flux data cover the range from 300 to 1050 nm. For some stars observed with the IUE orbiting observatory, the fluxes are available down to 150–170 nm. The energy distribution curves are given in the absolute-relative form, i.e. they all are normalized to 100 at 550 nm. The mean energy distribution of each star is given in the intensities per unit wavelength interval. Each value given in the catalog is the intensity integral in the interval $\Delta\lambda = 5$ nm centered on a given wavelength. The stars affected by interstellar extinction, are dereddened. The accuracy of the observed energy distributions will be estimated in the last section of this paper.

In the catalog of Sviderskienė (1992), Table 4 on pages 44–48 has a typographic error – the numbers of stars are given in wrong positions. The right order of HD numbers in the heading of the Table should be: HD 127665, 135722, 216763, 217906, 219615 and 2857 (instead of 217906, 219615, 2857, 127665, 135722 and 216763).

3. A COMPARISON OF THE MODEL AND THE OBSERVED SPECTRA

For the present investigation we have selected only the stars with extreme metal-deficiency: 6 blue horizontal-branch stars, 11

extreme subdwarfs and 6 extreme metal-deficient giants. These stars are listed in Table 1.

Effective temperatures, gravities and metallicities for most of these stars are taken from Cenarro et al. (2001) where these parameters are reduced to a unique system based on high-dispersion spectral analysis. According to that paper, the estimated errors of the parameters are ± 100 K for T_e , ± 0.2 dex for $\log g$ and ± 0.15 dex for $[\text{Fe}/\text{H}]$. For some stars the parameters are taken from other sources listed in the Notes to Table 1.

Sviderskienė (1992) has excluded the interstellar extinction effect on energy distribution curves for some giants which were found to be slightly reddened. We have made a new search of interstellar reddenings for the stars of Table 1. The values of color excesses, given in the Table, were used to deredden energy distributions of the stars. Intrinsic energy distributions $I_0(\lambda)$ were calculated from the observed $I(\lambda)$ by the equation

$$I_0(\lambda) = \frac{I(\lambda)}{\tau^x(\lambda)}, \quad (1)$$

where $\tau(\lambda)$ is the transmittance function of the unit mass of interstellar dust and x is the amount of unit masses. The values of x for different color excesses were calculated by the equation

$$x = \frac{E_{B-V}}{E_{B-V}^{(x=1)}}. \quad (2)$$

Here $E_{B-V}^{(x=1)}$ for stars of various spectral types are calculated from the standard interstellar extinction law $\tau(\lambda)$ given in Table 3 of the Straizys (1992) monograph using the following equations:

$$A_m = -2.5 \log \frac{\int I(\lambda) R_m(\lambda) \tau^x(\lambda) d\lambda}{\int I(\lambda) R_m(\lambda) d\lambda}. \quad (3)$$

and

$$E_{m_1-m_2} = A_{m_1} - A_{m_2}. \quad (4)$$

Here $I(\lambda)$ are the intrinsic energy distribution functions of stars, $R_m(\lambda)$ are the response functions of the B and V passbands, m_1 and m_2 are B and V magnitudes. Mean energy distribution functions for stars of various spectral classes were taken from Straizys &

Sviderskienė (1972) with the slightly revised ultraviolet. The values of $E_{B-V}^{(x=1)}$ due to the band-width effect slightly depend on the intrinsic energy distribution of the star: for O–B–A stars (including BHB stars) it is close to 1.00 and for the G5–K5 giants (including MDG stars) it is ~ 0.85 .

For the stars, which were dereddened by Sviderskienė, only differential reddening due to different color excess value was taken into account.

Figures 1–23 compare the energy distribution curves of Kurucz and Sviderskienė for the metal-deficient stars of Table 1. The temperatures of the models are rounded to the nearest number multiple of 10. For each star two Kurucz energy curves are plotted with the temperatures ± 200 K from the right value. The space between these two curves is shown in grey. The synthetic curves for the specific T_e , $\log g$ and $[\text{Fe}/\text{H}]$ are obtained by linear interpolation between the grid curves given by Kurucz. The following conclusions can be made for different types of stars.

(1) For the BHB stars the coincidence of energy distributions is relatively good. However some stars show considerable differences in some spectral ranges. For example, the model of HD 60778 (Figure 2) is stronger by 10–20% in the ultraviolet and violet and fainter by $\sim 5\%$ in the red and infrared. This difference can be corrected by taking a lower value of T_e of the star. The model energy curve of HD 161817 (Figure 6) is also higher by $\sim 10\%$ in the ultraviolet and violet, but no difference is seen in long wavelengths.

(2) In case of the extreme subdwarfs the coincidence is relatively good in the whole spectral range (from the ultraviolet to the infrared) only for HD 25329 (Figure 8) and BD+26 2606 (Figure 16). For the remaining nine subdwarfs the model curves, corresponding to the T_e values given in Table 1, are too low by 10–15% in the blue, violet and ultraviolet ranges. These differences cannot be explained by a T_e error, since in the red and infrared the model and the observed curves are close to each other. Only for HD 19445 (Figure 7) an increase in the temperature of the star by 200 K would force the observed and the model curves to be in sufficient agreement.

(3) For the extreme metal-deficient giants the coincidence of the observed and model curves in the red and infrared is also good. For HD 2665 (Figure 18) and HD 165195 (Figure 22) the model curve is good also in the violet and ultraviolet. However, for the other four stars there are systematic differences in the short wavelength part of

Table 1. A list of the stars whose spectral energy distribution data are compared with the Kurucz models.

| HD, BD | T_e | $\log g$ | [Fe/H] | E_{B-V} |
|----------------------------|-------|----------|--------|-----------|
| BHB stars | | | | |
| 2857 | 7563 | 2.67 | -1.60 | 0.02 |
| 60778 ^a | 8690 | 3.30 | -0.50 | 0.01 |
| 74721 ^b | 8640 | 3.55 | -1.48 | 0.01 |
| 86986 ^b | 7850 | 3.10 | -1.81 | 0.02 |
| 109995 | 8034 | 2.98 | -1.55 | 0.00 |
| 161817 | 7639 | 2.96 | -0.95 | 0.01 |
| F-G-K subdwarfs | | | | |
| 19445 | 5918 | 4.35 | -2.05 | 0.00 |
| 25329 | 4787 | 4.58 | -1.72 | 0.00 |
| 64090 ^c | 5446 | 4.45 | -1.76 | 0.00 |
| 84937 | 6228 | 4.01 | -2.17 | 0.00 |
| 94028 | 5941 | 4.21 | -1.49 | 0.00 |
| 103095 | 5025 | 4.56 | -1.36 | 0.00 |
| 140283 | 5687 | 3.55 | -2.53 | 0.01 |
| 188510 | 5490 | 4.69 | -1.59 | 0.00 |
| 219617 | 5878 | 4.04 | -1.39 | 0.00 |
| +26 2606 ^d | 6146 | 4.23 | -2.29 | 0.01 |
| +17 4708 | 6005 | 4.01 | -1.74 | 0.01 |
| G-K metal-deficient giants | | | | |
| 2665 | 5013 | 2.35 | -1.96 | 0.06 |
| 6755 | 5102 | 2.40 | -1.41 | 0.04 |
| 88609 | 4513 | 1.26 | -2.64 | 0.02 |
| 122563 | 4566 | 1.12 | -2.63 | 0.01 |
| 165195 | 4471 | 1.11 | -2.15 | 0.15 |
| 221170 ^c | 4465 | 1.04 | -2.10 | 0.03 |

NOTES:

^a HD 60778: parameters are from Danford & Lea (1981).^b HD 74721 and HD 86986: parameters are from Adelman & Philip (1994).^c HD 64090 and HD 221170: parameters are from Soubiran et al. (1998).^d BD +26 2606: parameters are from Gratton et al. (1996).

the spectrum: there is a general weakening of model spectra in the violet and ultraviolet for HD 6755, HD 88609, HD 122563 and HD 221170. The upper limit of the shadowed area in short wavelengths almost coincides with the real energy curve for all these four stars. This might indicate that T_e accepted for the stars is by ~ 200 K too low. However, acceptance of higher temperature will lead to a disagreement of energy curves in the red and infrared.

For the evaluation of the effect of gravity uncertainties, we have chosen three stars, representing BHB, SD and MDG stars. The value of $\log g$ was varied by ± 0.3 dex from the true value, keeping the T_e and $[\text{Fe}/\text{H}]$ values constant. Model energy curves for these stars are compared with the observed energy curves in Figures 24–26. It is evident that the gravity effects are of minor importance and they cannot help to explain the differences seen in Figs. 1–23. The same is true in the case of $[\text{Fe}/\text{H}]$ variations by ± 0.3 dex (Figures 27–29).

4. A COMPARISON OF SYNTHETIC COLOR INDICES

For a quantitative evaluation of the differences between the model and the observed energy distributions, we calculated and intercompared synthetic color indices in the *Vilnius* photometric system and the *UBV* system of the metal-deficient stars from Table 1 and the stars of luminosities V and III of solar chemical composition (hereafter, normal stars). The method of synthetic photometry used is described by Straizys (1996). Energy distributions for normal stars were taken from Straizys & Sviderskienė (1972) (with the corrected ultraviolet, as described in Paper I) and for metal-deficient stars – from Sviderskienė (1992). The response functions of the *Vilnius* and *UBV* systems were taken from Straizys (1992).

The results are shown in Figs. 30–37, where the differences Δ of corresponding color indices (“model” minus “observed”) are plotted against the effective temperatures. The temperatures for metal-deficient stars are taken from Table 1 and for the normal stars – from Paper I.

Synthetic color indices reflect the differences seen in energy distributions. For stars of solar chemical composition (dots and crosses) the scatter of stars gradually increases with decreasing temperature. However, for stars with $T_e > 4500$ K the deviations Δ do not exceed ± 0.2 mag even in case of color indices containing the ultraviolet magnitudes. The deviations of subdwarfs are also within these limits. The largest deviations (plus 0.3–0.4 mag) are observed for the

three coolest metal-deficient giants with the temperatures near 4500 K. It is probable, that in the ultraviolet these stars are really brighter than their Kurucz models.

5. DISCUSSION AND CONCLUSIONS

The comparison of energy distributions of real stars and their models, described in the previous sections, is a difficult problem for interpretation since there are several causes affecting the accuracy of the results. They are: (1) accidental and systematic errors of the observed energy distributions, (2) systematic errors in the account of opacity sources in model stellar atmospheres, and (3) errors of the accepted effective temperatures of the stars. Let us discuss these error sources separately.

When we plot energy distributions of a star, determined by different authors, and normalize all of them at one wavelength, say at 550 nm, then we find a considerable scatter of individual determinations at both ends of the wavelength interval covered. If we limit ourselves with the traditional ground-based data, covering the wavelengths between 320 nm and 1 μm , then the usual scatter of the energy flux values for G–K–M type stars is: $\pm 5\text{--}10\%$ at 350 nm and $\pm 5\%$ at 1 μm (Straižys & Sviderskienė 1972, Sviderskienė 1988). The flux values obtained as averages from the results of several authors should be more accurate.

A good test of the accuracy of the average spectral energy curves is a comparison of color indices obtained from these curves by synthetic photometry and color indices of the same stars observed photoelectrically with sufficiently high accuracy (± 0.01 mag). Such a comparison in the passbands of the *Vilnius* photometric system has been done both for normal stars of various luminosities (Sviderskienė 1988) and for metal-deficient stars (Sviderskienė 1992). In both cases the stars exhibit differences between the ultraviolet synthetic and observed color indices within ± 0.10 mag. Consequently, a considerable part of the differences seen in Figures 1–37 can be explained by the errors in observed energy distributions.

It is strange enough that the differences of the observed and the model energy distributions give an evidence that at least part of metal-deficient stars (subdwarfs and giants) exhibit overestimation of opacity in stellar atmospheres. It is more usual that synthetic spectra of model atmospheres demonstrate a “missing opacity”. On

the other hand, some model stars exhibit a perfect coincidence of their spectral energy distributions with observations. If the opacity were a problem, then all stars of a given type would behave in the same way.

The errors of the accepted effective temperatures is the third possibility. Although Cenarro et al. (2001) estimate their temperatures to be accurate within ± 100 K, it is not excluded that in some cases these errors may be twice larger. The vertical bars in Figures 35–37 show how the temperature errors of ± 200 K affect the plotted differences of color indices. It seems that these error bars are capable to explain the scatter of most stars in these figures, except of the stars cooler than ~ 4500 K.

Thus we conclude that the present investigation gives evidence that spectral energy distributions of the Kurucz metal-deficient models of the effective temperatures > 4500 K do not contradict the observed energy distributions of real stars belonging to the blue horizontal branch, extreme subdwarfs and extreme metal-deficient giants, if we take into account the errors of the observational data and of the effective temperatures. Cooler models probably exhibit some systematic differences in the ultraviolet and violet wavelengths.

ACKNOWLEDGMENT. We are grateful to A. G. Davis Philip for his important comments.

REFERENCES

- Adelman S. J., Philip A. G. D. 1994, MNRAS, 269, 579
 Cenarro A. J., Gorgas J., Cardiel N., Pedraz S., Peletier R. F., Vazdekis A. 2001, MNRAS, 326, 981
 Danford S. C., Lea S. M. 1981, AJ, 86, 1909
 Gratton R. G., Carretta E., Castelli F. 1996, A&A, 314, 191
 Kurucz R. L. 1995, personal communication
 Soubiran C., Katz D., Cayrel R. 1998, A&AS, 133, 221
 Straizys V. 1992, Multicolor Stellar Photometry, Pachart Publishing House, Tucson, Arizona
 Straizys V. 1996, Baltic Astronomy, 5, 459
 Straizys V., Liubertas R., Valiauga G. 1997, Baltic Astronomy, 6, 601 (Paper I)
 Straizys V., Sviderskienė Z. 1972, Bull. Vilnius Obs., No. 35, 3
 Sviderskienė Z. 1988, Bull. Vilnius Obs., No. 80, 3
 Sviderskienė Z. 1992, Bull. Vilnius Obs., No. 86, 3

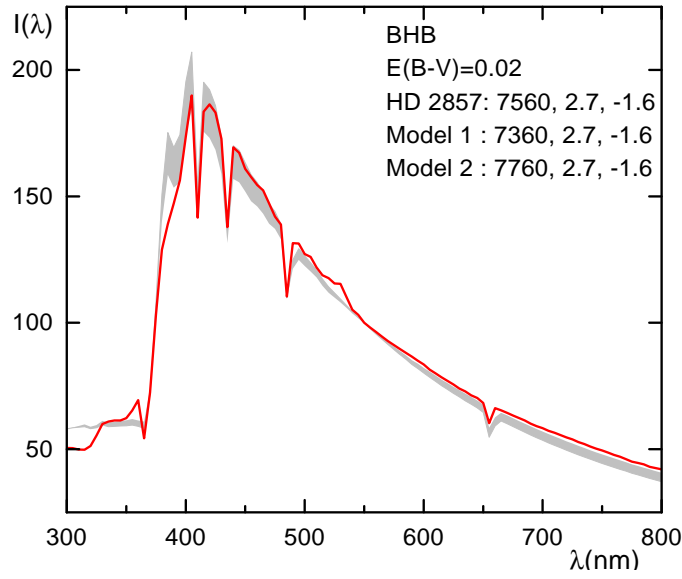


Fig. 1. Spectral energy distribution of HD 2857 (BHB star). The effective temperature of the model is changed by ± 200 K.

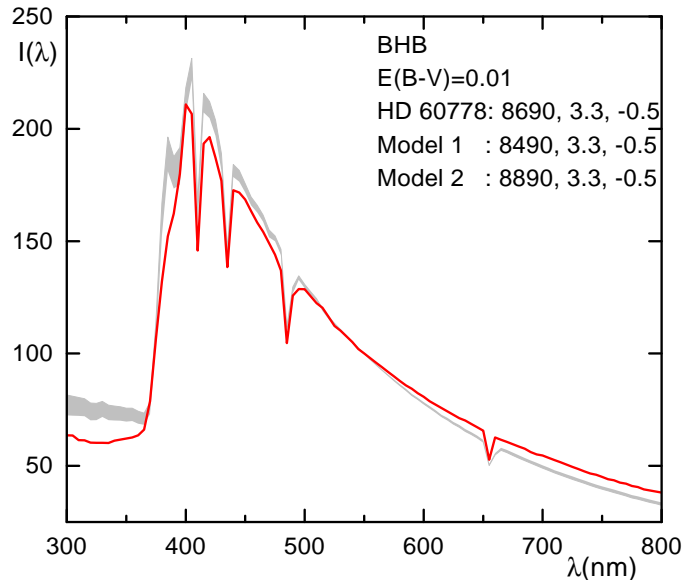


Fig. 2. Spectral energy distribution of HD 60778 (BHB star). The effective temperature of the model is changed by ± 200 K.

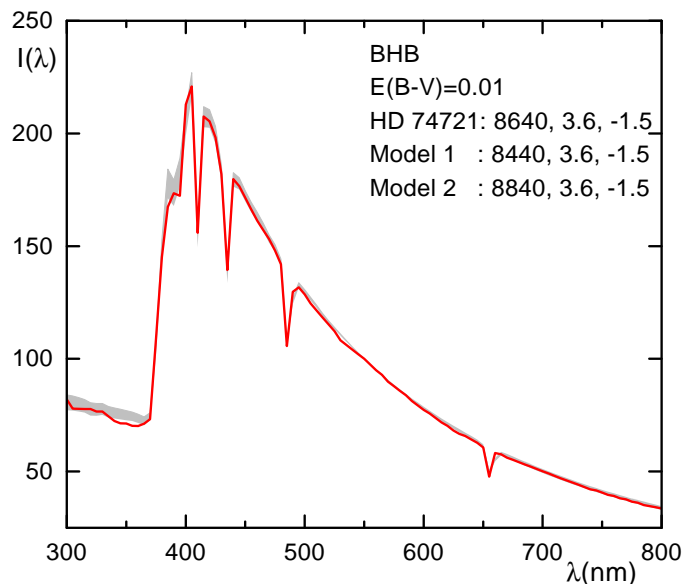


Fig. 3. Spectral energy distribution of HD 74721 (BHB star). The effective temperature of the model is changed by ± 200 K.

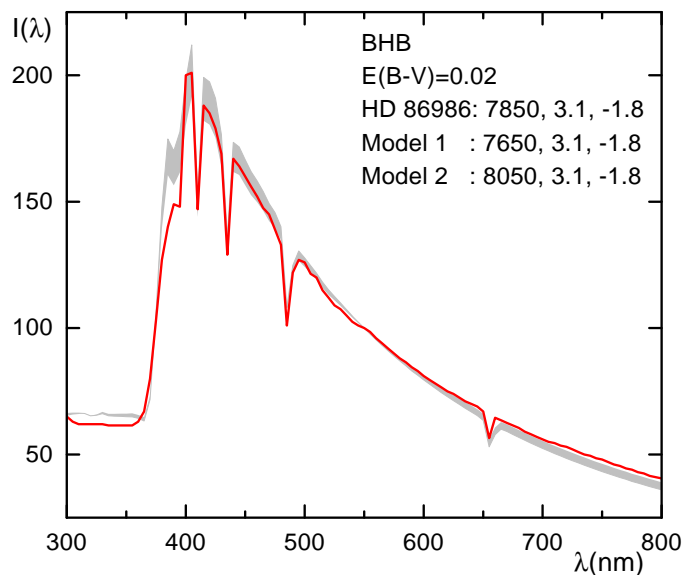


Fig. 4. Spectral energy distribution of HD 86986 (BHB star). The effective temperature of the model is changed by ± 200 K.

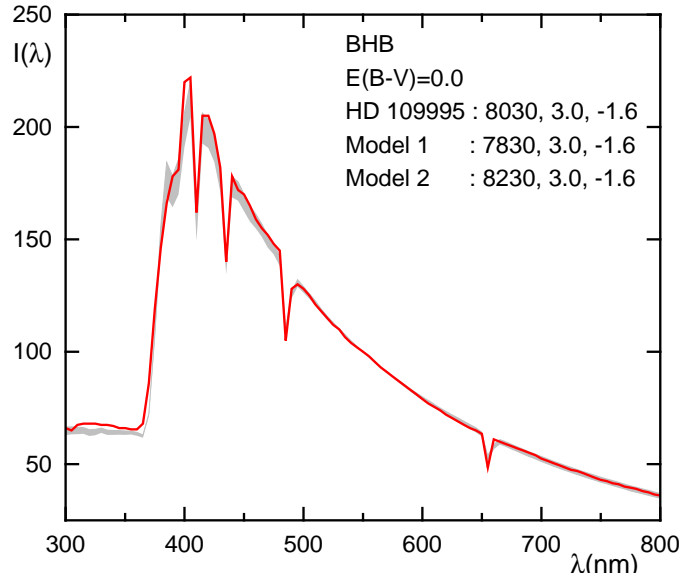


Fig. 5. Spectral energy distribution of HD 109995 (BHB star). The effective temperature of the model is changed by ± 200 K.

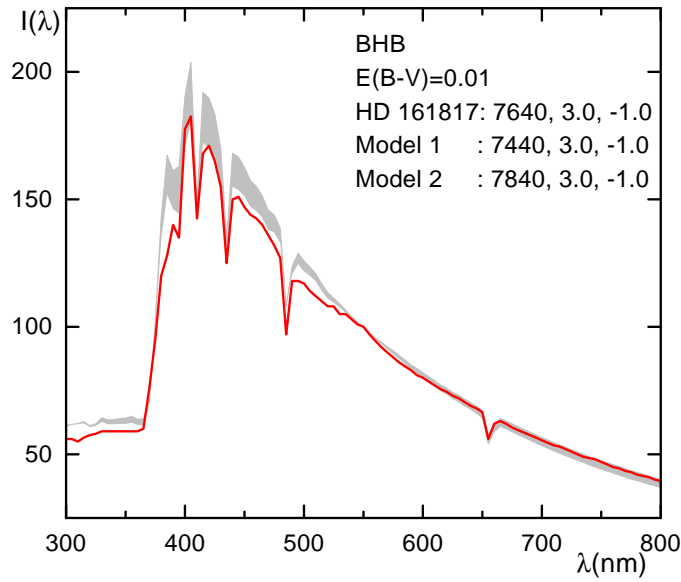


Fig. 6. Spectral energy distribution of HD 161817 (BHB star). The effective temperature of the model is changed by ± 200 K.

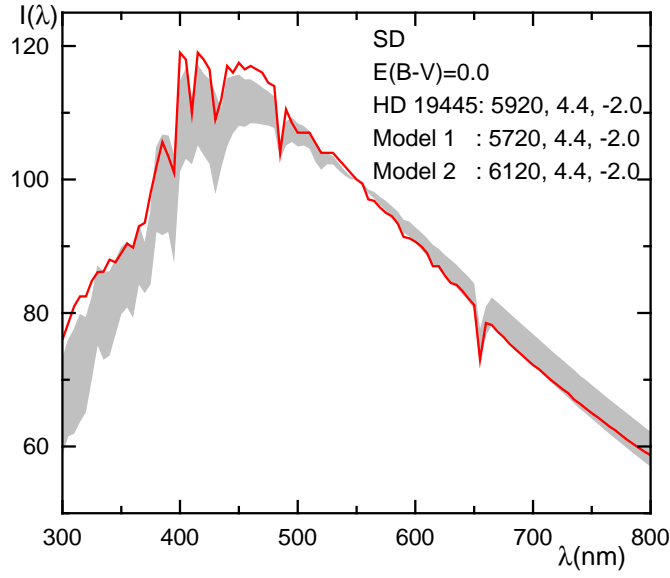


Fig. 7. Spectral energy distribution of HD 19445 (subdwarf). The effective temperature of the model is changed by ± 200 K.

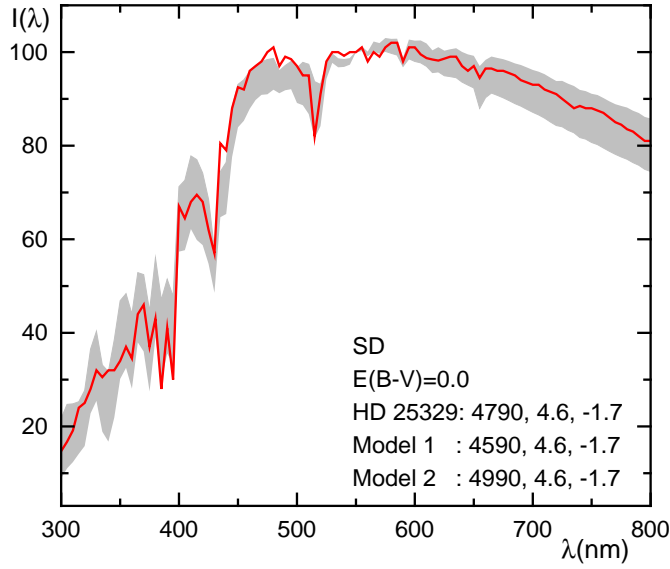


Fig. 8. Spectral energy distribution of HD 25329 (subdwarf). The effective temperature of the model is changed by ± 200 K.

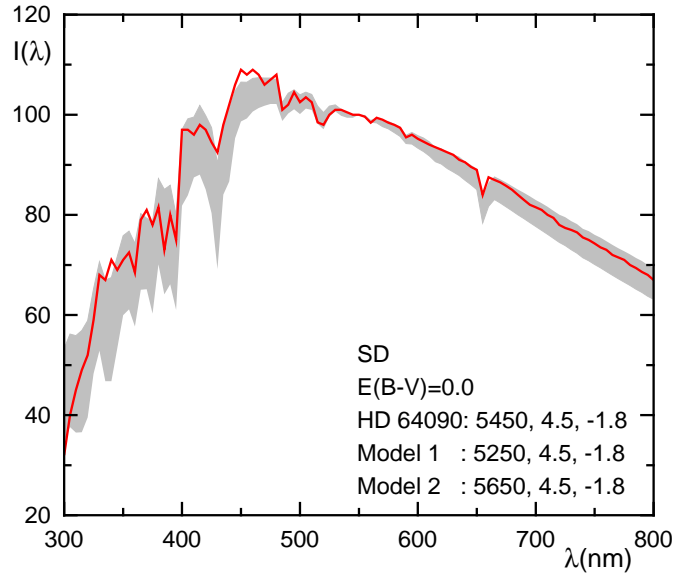


Fig. 9. Spectral energy distribution of HD 64090 (subdwarf). The effective temperature of the model is changed by ± 200 K.

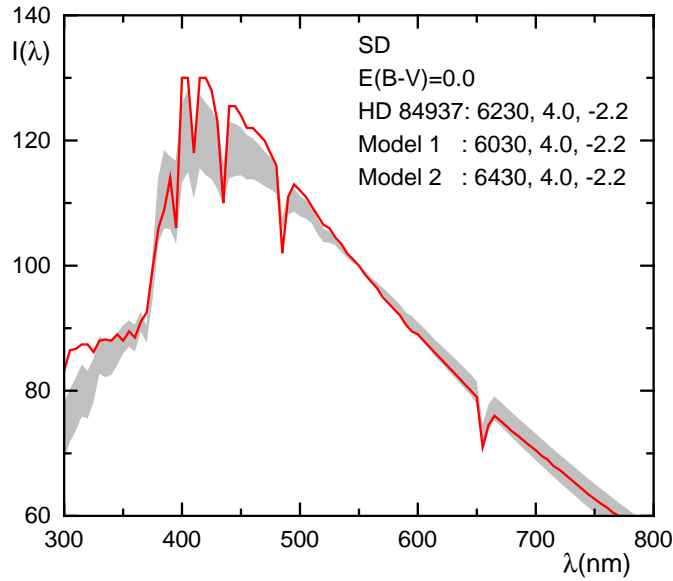


Fig. 10. Spectral energy distribution of HD 84937 (subdwarf). The effective temperature of the model is changed by ± 200 K.

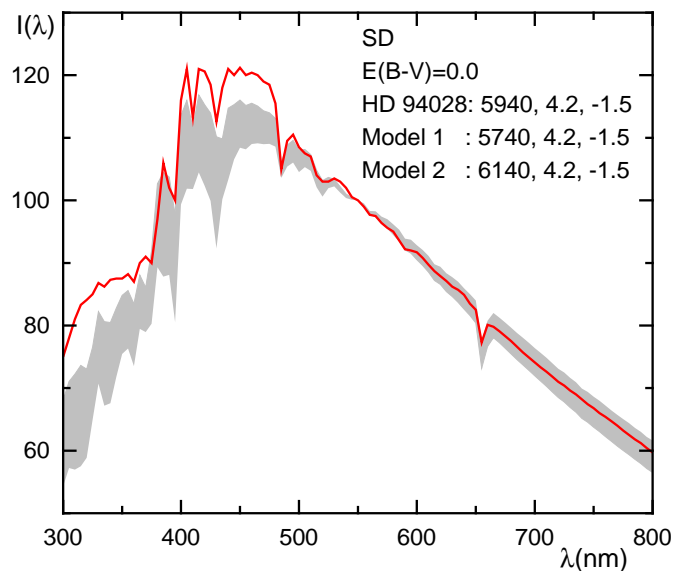


Fig. 11. Spectral energy distribution of HD 94028 (subdwarf). The effective temperature of the model is changed by ± 200 K.

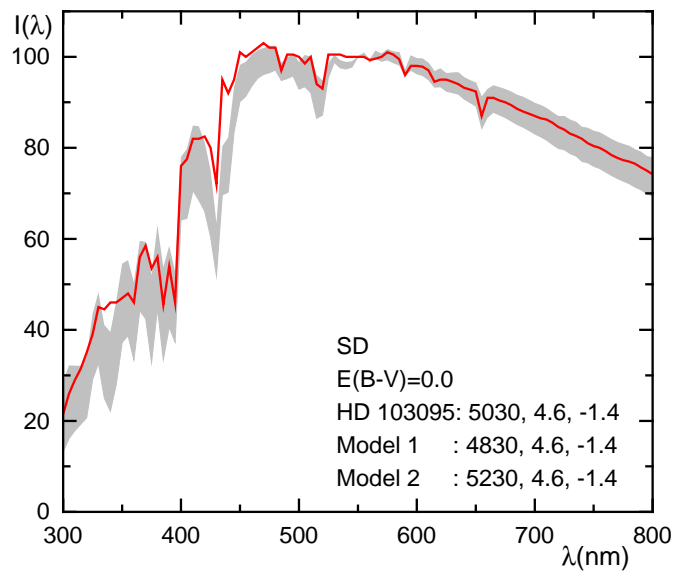


Fig. 12. Spectral energy distribution of HD 103095 (subdwarf). The effective temperature of the model is changed by ± 200 K.

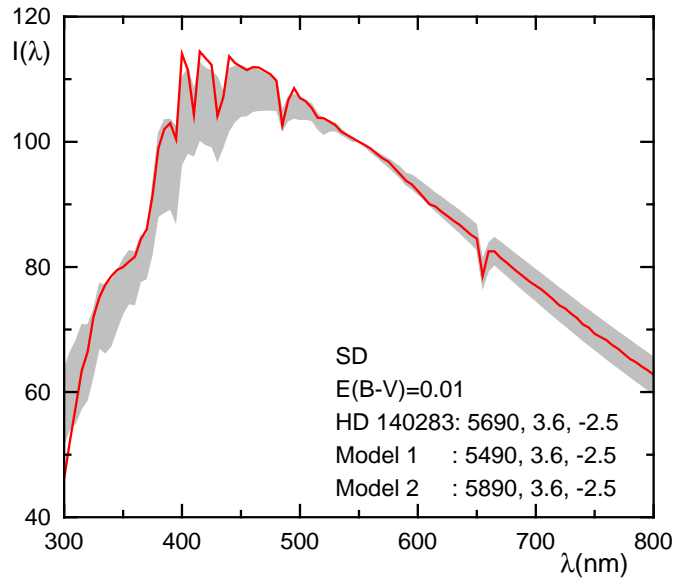


Fig. 13. Spectral energy distribution of HD 140283 (subdwarf). The effective temperature of the model is changed by ± 200 K.

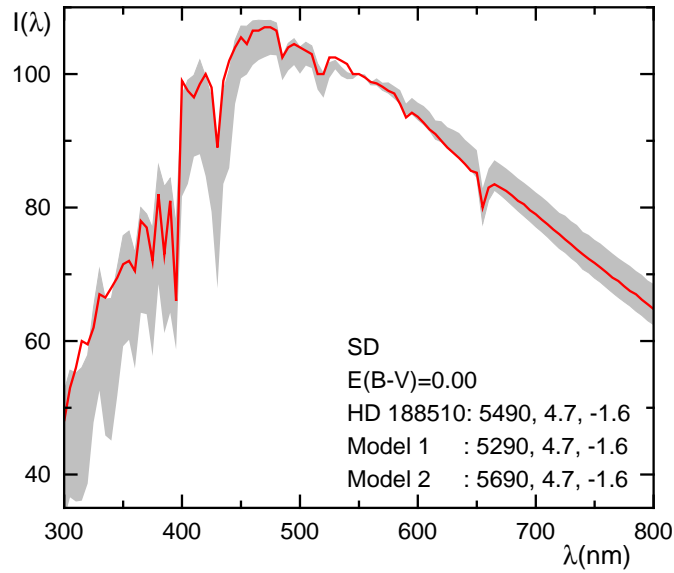


Fig. 14. Spectral energy distribution of HD 188510 (subdwarf). The effective temperature of the model is changed by ± 200 K.

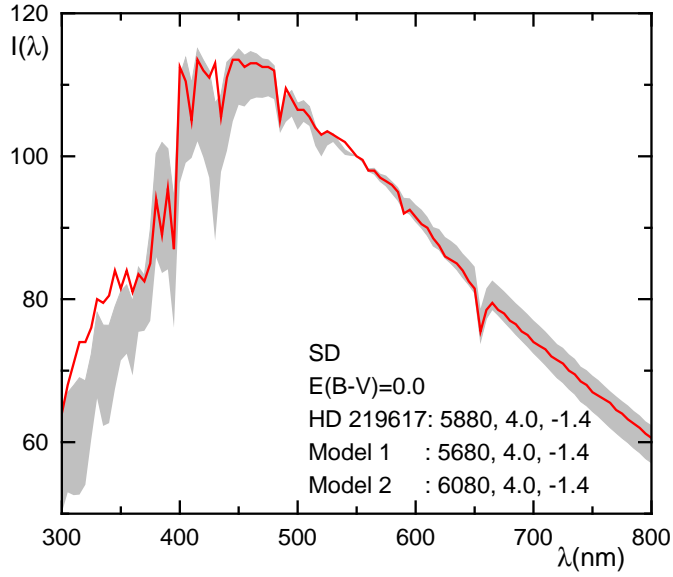


Fig. 15. Spectral energy distribution of HD 219617 (subdwarf). The effective temperature of the model is changed by ± 200 K.

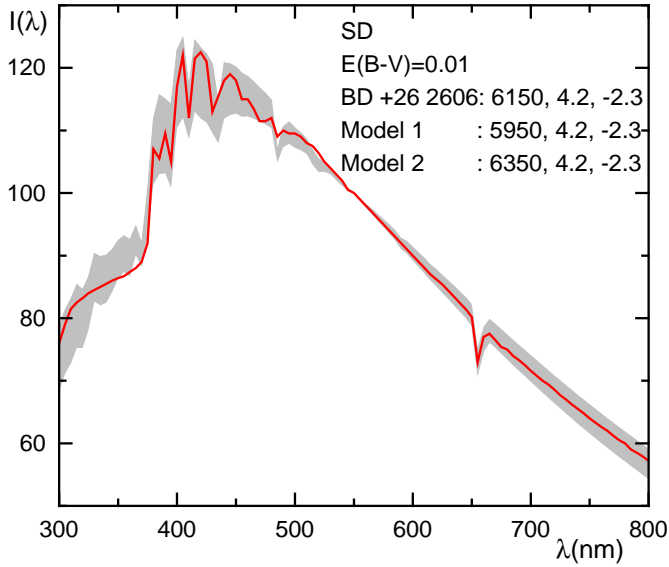


Fig. 16. Spectral energy distribution of BD+26 2606 (subdwarf). The effective temperature of the model is changed by ± 200 K.

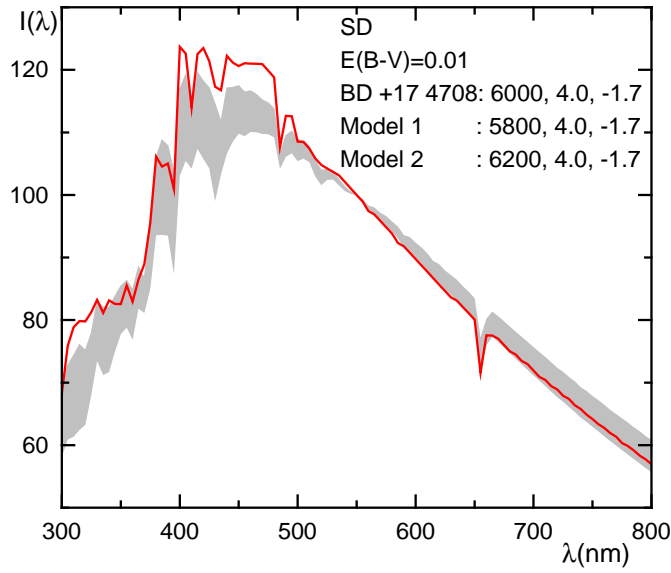


Fig. 17. Spectral energy distribution of BD+17 4708 (subdwarf). The effective temperature of the model is changed by ± 200 K.

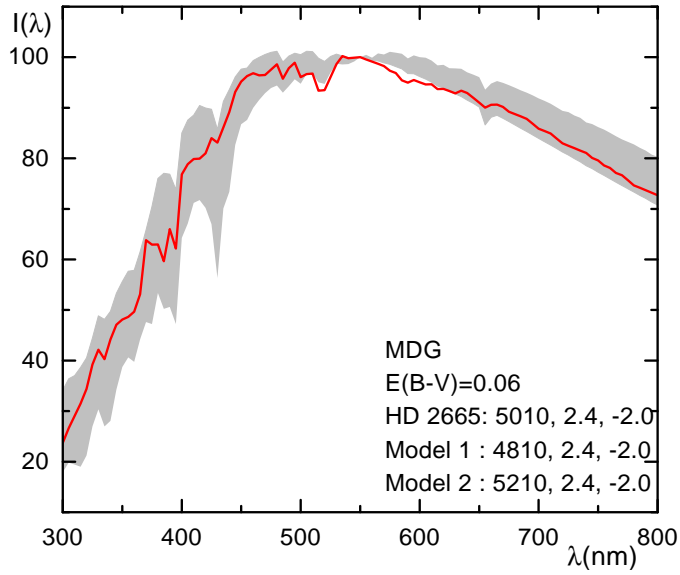


Fig. 18. Spectral energy distribution of HD 2665 (MD giant). The effective temperature of the model is changed by ± 200 K.

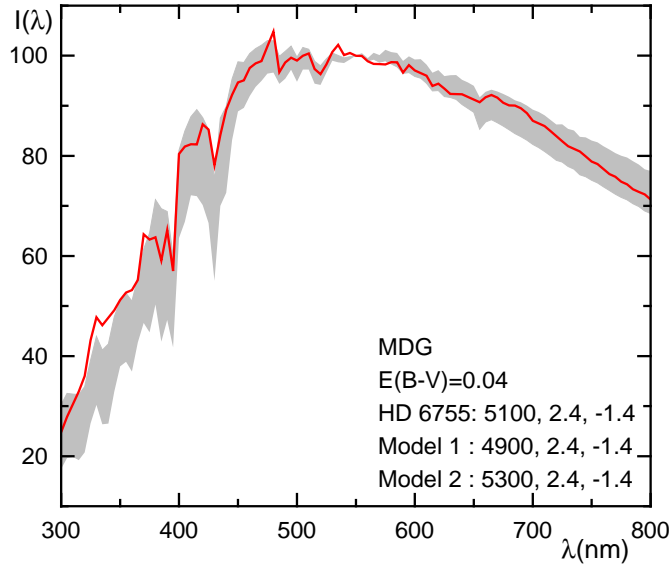


Fig. 19. Spectral energy distribution of HD 6755 (MD giant). The effective temperature of the model is changed by ± 200 K.

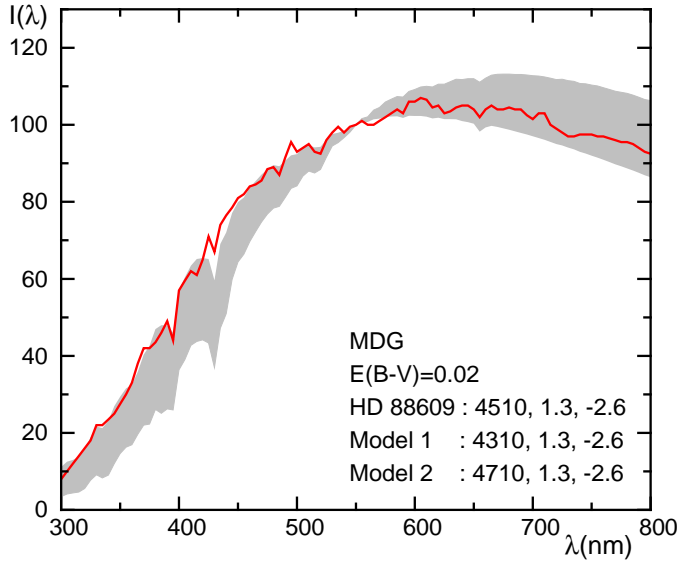


Fig. 20. Spectral energy distribution of HD 88609 (MD giant). The effective temperature of the model is changed by ± 200 K.

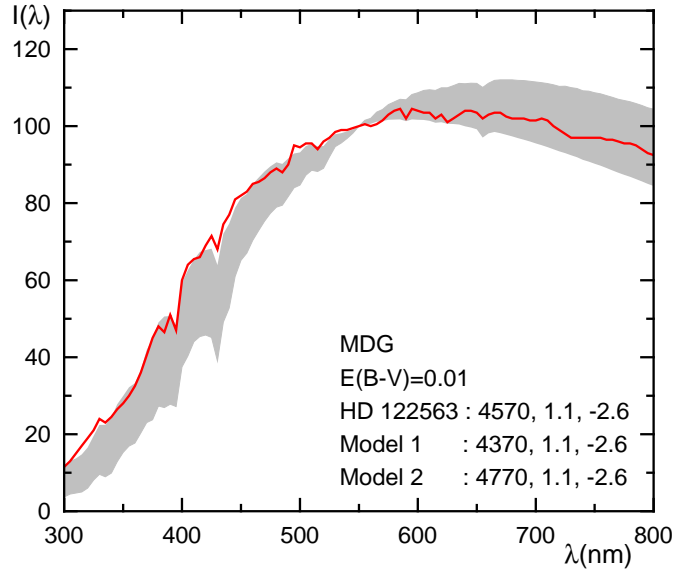


Fig. 21. Spectral energy distribution of HD 122563 (MD giant). The effective temperature of the model is changed by ± 200 K.

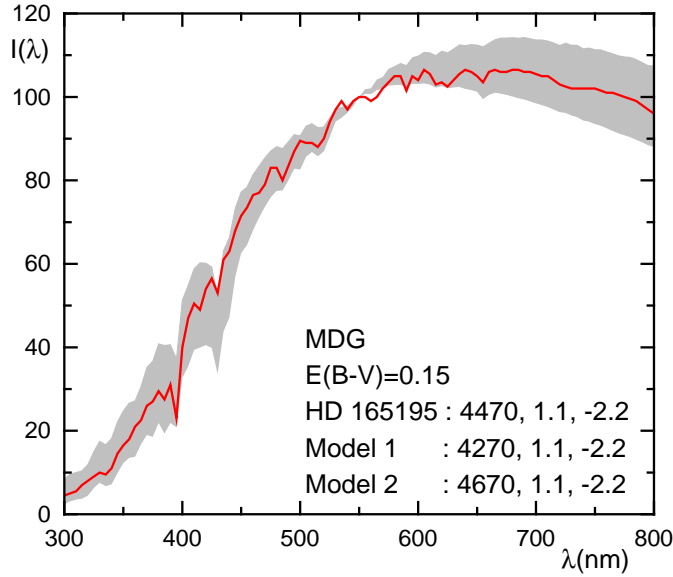


Fig. 22. Spectral energy distribution of HD 165195 (MD giant). The effective temperature of the model is changed by ± 200 K.

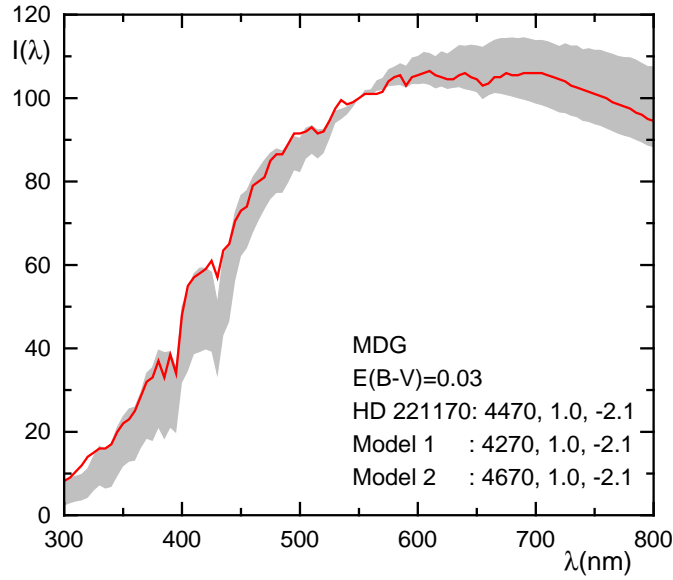


Fig. 23. Spectral energy distribution of HD 221170 (MD giant). The effective temperature of the model is changed by ± 200 K.

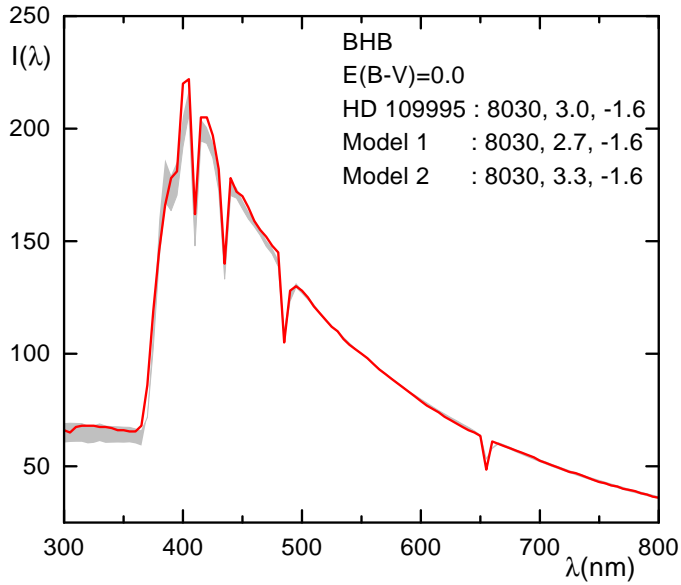


Fig. 24. Spectral energy distribution of HD 109995 (BHB star). The gravity of the model is changed by ± 0.3 dex.

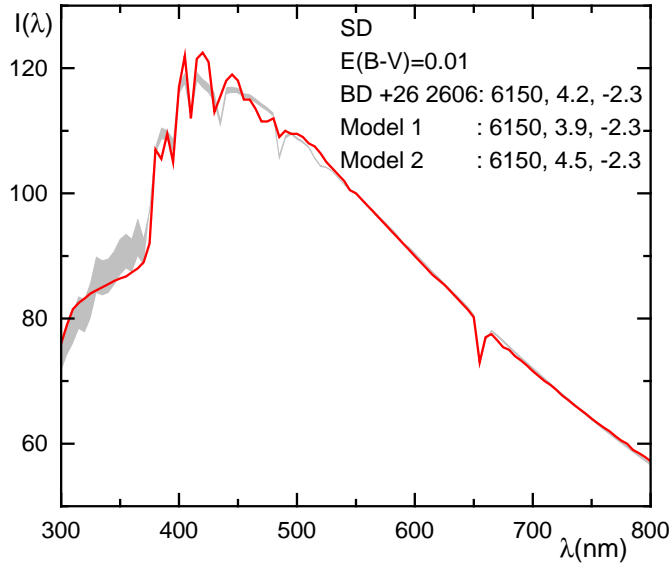


Fig. 25. Spectral energy distribution of BD+26 2606 (subdwarf). The gravity of the model is changed by ± 0.3 dex.

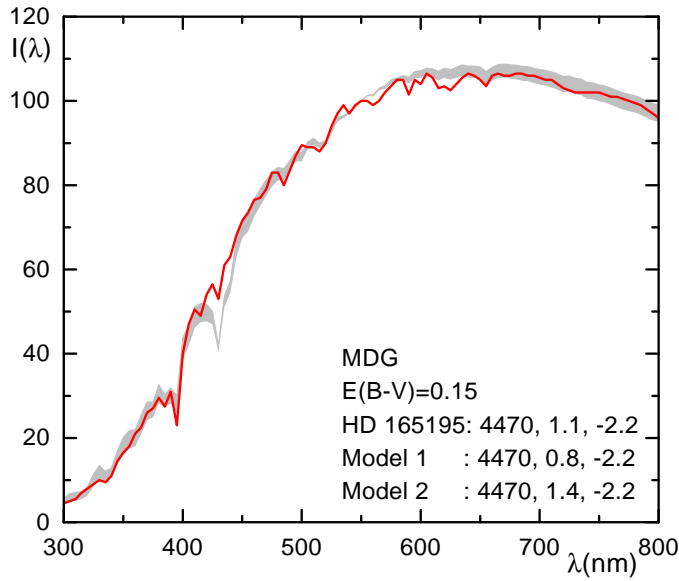


Fig. 26. Spectral energy distribution of HD 165195 (MD giant). The gravity of the model is changed by ± 0.3 dex.

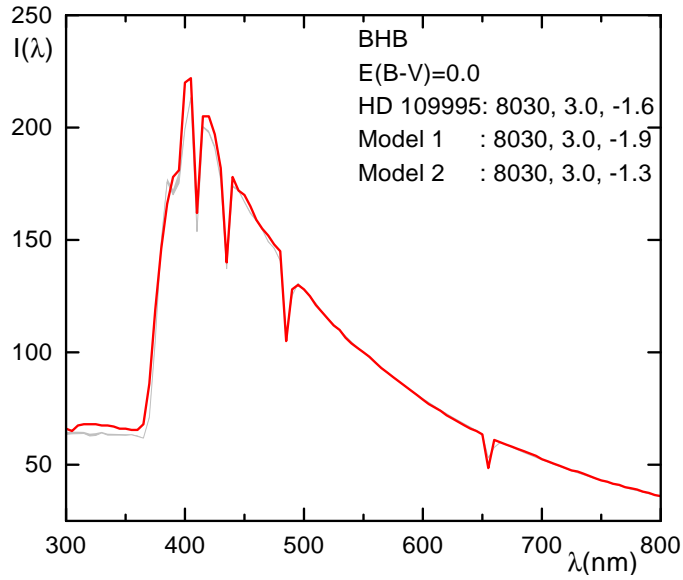


Fig. 27. Spectral energy distribution of HD 109995 (BHB star). The metallicity of the model is changed by ± 0.3 dex.

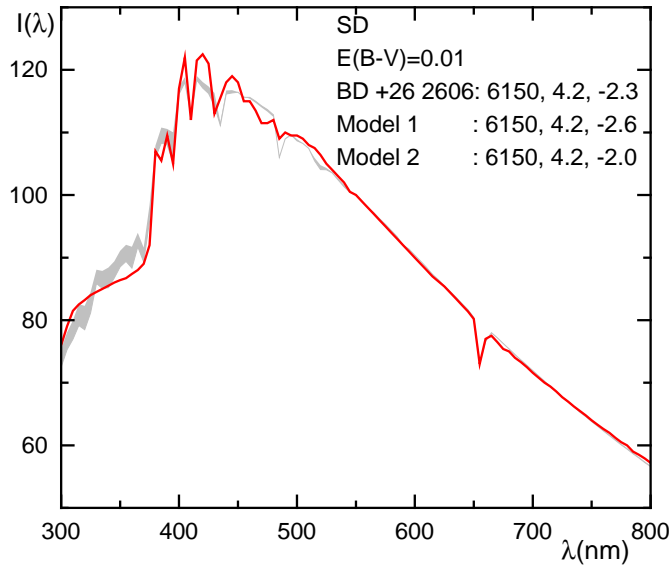


Fig. 28. Spectral energy distribution of BD+26 2606 (subdwarf). The metallicity of the model is changed by ± 0.3 dex.

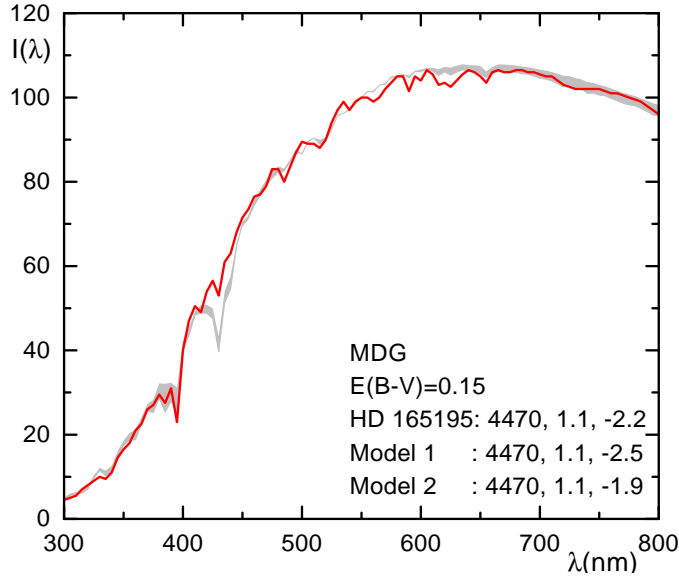


Fig. 29. Spectral energy distribution of HD 165195 (MD giant). The metallicity of the model is changed by ± 0.3 dex.

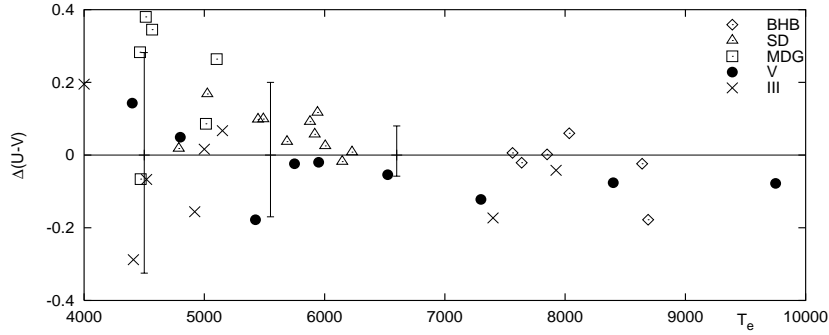


Fig. 30. A comparison of the $U-V$ color indices of stars and their models (model minus observed). Mean wavelengths of the U and V passbands are 345 and 544 nm. The vertical bars indicate the errors originating from the temperature changes by ± 200 K.

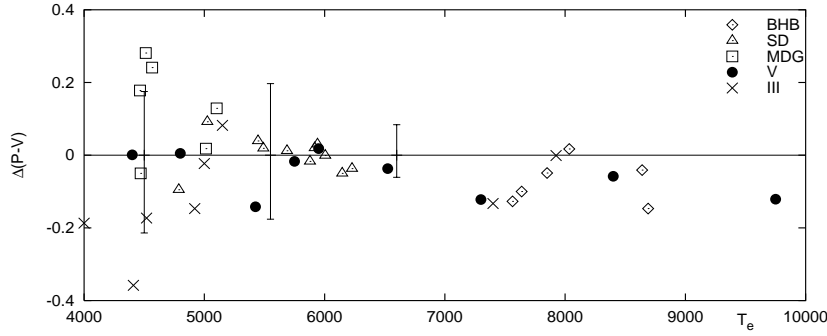


Fig. 31. The same as in Fig. 30 but for $P-V$. The mean wavelength of the P passband is 375 nm.

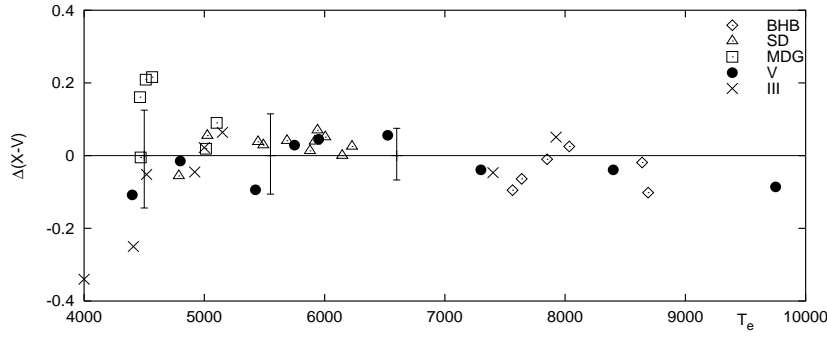


Fig. 32. The same as in Fig. 30 but for $X-V$. The mean wavelength of the X passband is 405 nm.

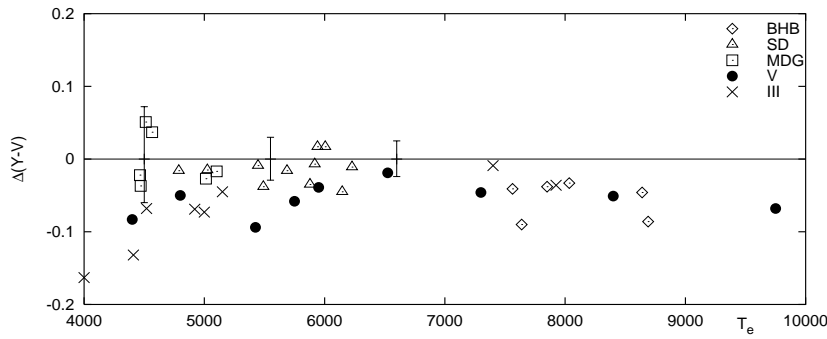


Fig. 33. The same as in Fig. 30 but for $Y-V$. The mean wavelength of the Y passband is 466 nm.

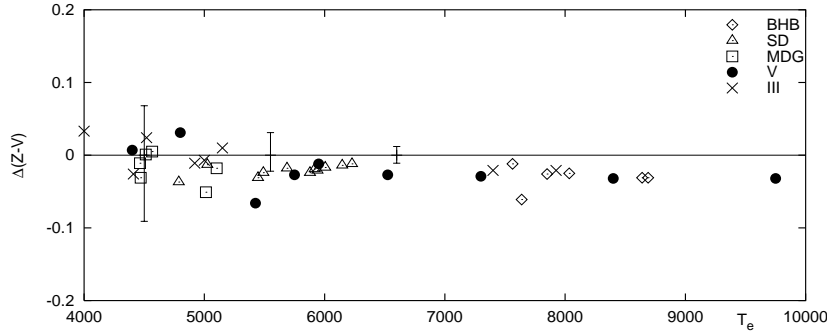


Fig. 34. The same as in Fig. 30 but for $Z-V$. The mean wavelength of the Z passband is 516 nm.

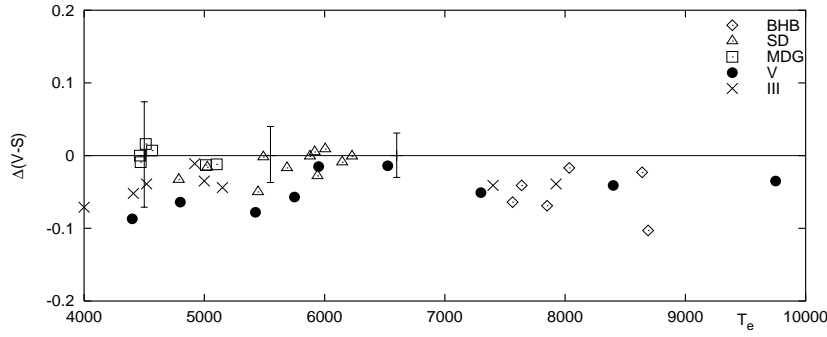


Fig. 35. The same as in Fig. 30 but for $V-S$. The mean wavelength of the S passband is 656 nm.

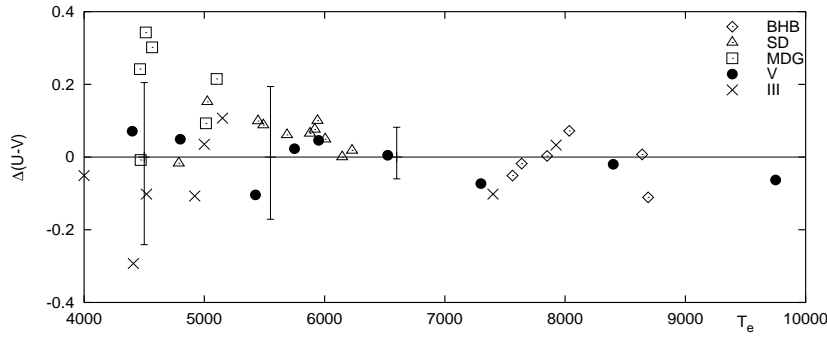


Fig. 36. The same as in Fig. 30 but for $U-V$ of the UBV system. Mean wavelengths of the U and V passbands are 364 and 550 nm.

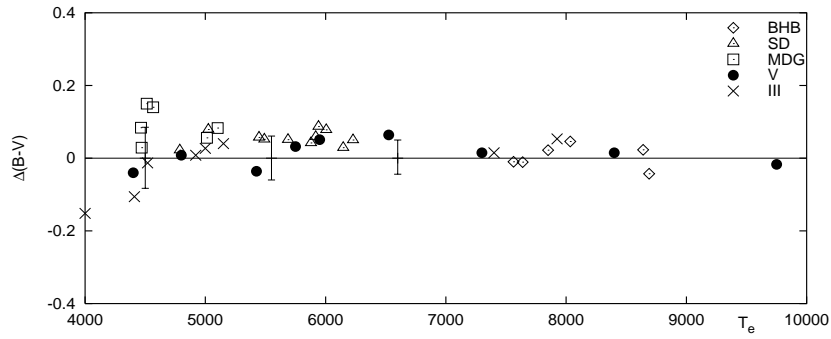


Fig. 37. The same as in Fig. 30 but for $B-V$ of the UBV system. The mean wavelength of the B passband is 442 nm.